Molecular Therapy
Methods & Clinical Development
Original Article

Efficacy and muscle safety assessment of fukutin-related protein gene therapy

Halli Benasutti,[1,2,12] Joseph W. Maricelli,[3,4,12] Jane Seto,[2,5,9,12] John Hall,[2,10] Christine Halbert,[2,5] Jacqueline Wicki,[2] Lydia Heusgen,[2] Nicholas Purvis,[2] Michael Regnier,[6] David C. Lin,[7] Buel D. Rodgers,[3,4,11] and Jeffrey S. Chamberlain[1,2,5,8]

[1]Department of Biochemistry, University of Washington School of Medicine, Seattle, WA, USA; [2]Department of Neurology, University of Washington School of Medicine, Seattle, WA, USA; [3]School of Molecular Biosciences, Washington State University College of Veterinary Medicine, Pullman, WA 99164, USA; [4]Washington Center for Muscle Biology, Washington State University, Pullman, WA 99164, USA; [5]Sen. Paul D. Wellstone Muscular Dystrophy Specialized Research Center, University of Washington School of Medicine, Seattle, WA, USA; [6]Department of Bioengineering, University of Washington School of Medicine, Seattle, WA, USA; [7]Department of Integrative Physiology and Neuroscience and the Voiland School of Chemical Engineering and Bioengineering, Washington State University, Pullman, WA 99164, USA; [8]Department of Medicine, University of Washington School of Medicine, Seattle, WA, USA

Limb-girdle muscular dystrophy type R9 (LGMDR9) is a muscle-wasting disease that begins in the hip and shoulder regions of the body. This disease is caused by mutations in fukutin-related protein (FKRP), a glycosyltransferase critical for maintaining muscle cell integrity. Here we investigated potential gene therapies for LGMDR9 containing an FKRP expression construct with untranslated region (UTR) modifications. Initial studies treated an aged dystrophic mouse model ($FKRP^{P448L}$) with adeno-associated virus vector serotype 6 (AAV6). Grip strength improved in a dose- and time-dependent manner, injected mice exhibited fewer central nuclei and serum creatine kinase levels were 3- and 5-fold lower compared to those in non-injected $FKRP^{P448L}$ mice. Treatment also partially stabilized the respiratory pattern during exercise and improved treadmill running, partially protecting muscle from exercise-induced damage. Western blotting of C2C12 myotubes using a novel rabbit antibody confirmed heightened translation with the UTR modifications. We further explored the question of FKRP toxicity in wild-type mice using high doses of two additional muscle-tropic capsids: AAV9 and AAVMYO1. No toxic effects were detected with either therapeutic agent. These data further support the feasibility of gene therapy to treat LGMDR9.

INTRODUCTION

Dystroglycanopathies are a family of muscle disorders (>20)[1] that are caused by altered glycosylation of α-dystroglycan (α-DG), a peripheral membrane protein located on the extracellular side of the sarcolemma that normally binds to laminin. The laminin-α-DG association is a crucial portion of the dystrophin-glycoprotein complex (DGC), which provides a mechanical link between the intracellular actin cytoskeleton and the extracellular matrix. The DGC enables lateral transmission of forces from within myofibers,[2] allowing the muscle bundle to contract in unison and preventing cellular damage by internally maintained contractile energy. More than 11 glycosyltransferases are known to post-translationally modify α-DG,[3] working sequentially to build long glycan chains onto the protein. One such glycosyltransferase, Fukutin-related protein (FKRP), catalyzes the transfer of ribitol 5-phosphate to a phosphorylated O-mannosyl trisaccharide on α-DG, but only after fukutin has added a ribitol 5-phosphate to the growing chain. These sequential modifications lead up to addition of a repeating glucuronic acid and xylose chain[1] that serves as the laminin binding domain of α-DG.

Altered α-DG glycosylation severely disrupts the DGC mechanics, leading to fragile sarcolemma membranes and muscular dystrophy. These resulting dystroglycanopathies are the primary cause of several forms of congenital muscular dystrophy as well as multiple limb-girdle muscular dystrophies. Limb-girdle muscular dystrophy type R9 (LGMDR9, previously LGMD2I) is one of the most common of these diseases. It is an autosomal recessive disorder caused by mutations in the *FKRP* gene, which also can lead to congenital muscular dystrophy (MDC1C), Walker-Warburg syndrome (WWS), and muscle-eye-brain (MEB) disease. Our study is focused on developing treatment options for LGMDR9, although the results will also be relevant to the other, less prevalent FKRP disorders. LGMDR9 is slowly progressive, but patients still experience symptoms such as muscle weakness, muscle cramps, hypertrophy, joint contractures, and, in some cases, severe cardiomyopathy and respiratory issues. The age of LGMDR9 onset varies, with a spectrum of symptoms presenting in relation to specific mutations in FKRP.[4] For example, affected LGMDR9 patients are often wheelchair dependent by 25 years after

Received 28 November 2022; accepted 31 May 2023;
https://doi.org/10.1016/j.omtm.2023.05.022.

[9]Present address: Murdoch Institute, Melbourne, VIC, Australia

[10]Present address: Dyne Therapeutics, Waltham, MA 02451, USA

[11]Present address: AAVogen Inc., Rockville, MD 20850, USA

[12]These authors contributed equally

Correspondence: Jeffrey S. Chamberlain, PhD, University of Washington School of Medicine, 850 Republican St., Seattle, WA 98109-8055, USA.
E-mail: jsc5@uw.edu

age of onset. Diagnoses are typically made based on elevated serum creatine kinase (CK) levels and proximal muscle weakness followed by genotyping. There is no cure for LGMDR9, and treatments are limited to temporary symptom amelioration.

LGMDR9 is often due to heterozygous and homozygous mutations in the 1.5-kb coding region of the *FKRP* gene, the most common of which is 826C>A (L276I).[5] There is a strong genotype-phenotype correlation for this mutation, with compound heterozygous patients displaying a more severe phenotype than homozygous patients.[6] Another common mutation is 1343C>T (P448L), and both mutations interfere with the transfer of FKRP from the endoplasmic reticulum to the Golgi apparatus.[7] Because FKRP is a post-translational glycosyltransferase, mislocalization of this enzyme leads to decreased glycosylation and half-life and results in increased targeting of α-DG by the proteosome.[8] Additionally, other insertion, deletion, missense, and nonsense mutations have been reported in patients, although less commonly than the L276I and P448L point mutations. Interestingly, FKRP-null mutations are embryonic lethal,[9] which explains why all patients genotyped to date have at least one mutant allele that leads to expression of a presumably partially functional protein. These and other data[10] suggest that most, if not all, mutant FKRP enzymes found in patients still retain some enzymatic activity.

Developing approaches for gene therapy of LGMDR9 have been promising. However, inconsistent vectors, mouse age, genotype, and transgene have resulted in contradictory toxicity evidence associated with FKRP overexpression. For example, recent data have shown that adeno-associated virus (AAV) vector-mediated systemic delivery of FKRP can significantly ameliorate the dystrophic phenotype in a murine disease model, the $FKRP^{P448L}$ mouse.[11,12] By contrast, studies with a different model, the $FKTN^{-/-}$ mouse, suggest that muscle pathologies are exacerbated because central nucleation, endomysial fibrosis, and macrophage infiltration all increased with treatment.[13] Phenotypic differences in the mouse models are noticeable because $FKRP^{P448L}$ mice reasonably recapitulate LGMDR9,[14,15] while the $FKRP^{L276I}$ mouse displays a mild or less pronounced phenotype.[16,17] Mouse age varied widely across the studies and the regulatory cassettes used in the various studies similarly differed; some groups used the strong and ubiquitously expressed cytomegalovirus (CMV; human CMV immediate-early enhancer plus promoter) or CB (CMV enhancer/chicken β-actin promoter) cassettes, while others used a muscle-specific CK (CK7) cassette. Use of mouse vs. human FKRP cDNA also varied between studies as did doses that ranged from 2×10^{12} vector genomes (vg)/kg to 6×10^{13} vg/kg. The ability of gene therapy to treat LGMDR9 as well as its durability are also significantly dose dependent, with lower doses displaying shorter-term but still significant effects.[18]

Moreover, only one test of systemic muscle function has been performed on $FKRP^{P448L}$ mice receiving FKRP gene therapy: a treadmill exhaustion assay that, although useful, provides limited metrics for analysis. Other tests of systemic muscle function include running wheels for voluntary exercise and treadmills with respiratory chambers for assessing metabolic rate during forced exercise,[19] all of which are recommended assessments for preclinical studies with dystrophic mice.[20,21] Quantifying metabolic rate through indirect calorimetry assesses the combined functional integrity of skeletal and cardiac muscle and differs from plethysmography. This latter measure of ventilation reflects diaphragm function only and has little effect on metabolic rate.[22–26] Exercise-based assessments mimic those often used to assess dystrophic patients in the clinic (e.g., 6-min-walk test) and can be used to exacerbate the dystrophic phenotype in preclinical studies.[27–30]

The therapeutic delivery method is yet another critical component that must be considered in development of the safest possible therapeutic for LGMDR9 and related CMDs. Increased gene expression is often a critical part of gene therapy because therapeutic agents are limited by the immune responses associated with high doses of AAVs in human patients. For example, the issue of systemically administered AAVs and the accompanying liver toxicity seen in clinical trials[31,32] remain a barrier moving forward. Therefore, an ideal treatment would maximize gene expression while minimizing the AAV dose. The latest advancements in AAV vector design have led to increased targeting and gene expression in specific tissues. The development of these capsid variants that enable muscle-specific gene delivery may alter dosing thresholds and therapeutic efficacy[33–35] and need to be examined in relation to current vectors used in the clinic. One such novel AAV capsid has been named AAVMYO1 for its myotropic properties and has been shown to increase efficiency and specificity in heart, diaphragm, and skeletal muscle.[34] These new developments not only address the issue of myotropism but also decrease liver tropism, which will be critical to avoid the issues of innate immunity and will affect the success of gene therapies using high-dose AAV vectors.

While it has been shown that FKRP gene therapy is generally an effective treatment in mouse models for LGMDR9,[13,18] there has been little focus on transgene designs. Transgene optimization provides a tool to improve efficacy and lower necessary treatment doses. One such successful method of increasing gene expression was demonstrated in samples from cystic fibrosis patients.[36,37] The untranslated region (UTR) of the CFTR gene contains regulatory elements that decrease translation; in this case, formation of a secondary structure in the 5′ UTR post-transcriptionally regulates CFTR via cooperative regulatory effects. Thus, removal of the 5′ UTR ultimately increases CFTR expression. We discovered evidence of potential secondary structures in the UTRs of FKRP mRNA.[38] One particularly relevant structure is an RNA G-quadruplex (RGQ), a stable secondary mRNA configuration associated with inhibition of translation.[39,40] Repeats of a (CGG) motif in the 5′ UTR of FKRP are suggestive of an RGQ, and further investigation into UTRs may provide a tool for tunable gene expression (for FKRP and other genes).

The current study tested the dose-dependent efficacy of a novel FKRP gene therapy agent. This particular therapeutic agent differed from the vectors tested previously[11,13,16] because it used AAV6 instead of AAV9 as well as a miniaturized mouse muscle CK

enhancer/promoter (*CK8e*) that is uniquely active and specific for striated muscle (AAV6-Ck8e-humanFKRP [A6.C8hF]).[41–47] Furthermore, we examined a range of mouse ages and assessed systemic muscle function using a customized treadmill protocol.[30] Our results suggest that delivering a small FKRP cDNA to FKRPP448L mice significantly improves different aspects of striated muscle structure and function in a dose-dependent manner. However, even the higher dose tested here did not completely restore muscle function to levels seen in wild-type mice. Finally, to address the issue of potential FKRP toxicity, we explored whether overexpression of FKRP in wild-type mice affected muscle physiology. These studies delivered the small FKRP cDNA using multiple doses of vectors pseudotyped with capsids from AAV6,[48] AAV9,[49] and the newer myotropic AAVMYO1.[33] Cardiac and muscle physiology did not identify any adverse functional effects because of the exogenous FKRP in wild-type mice when delivered with any of these serotypes.

RESULTS

Removal of the UTRs from the FKRP cDNA increases protein expression

To explore FKRP expression, we initially generated a rabbit polyclonal antiserum (named Ab607) against a conserved fragment of the C terminus of mouse and human FKRP (materials and methods). To verify the utility of the antiserum after affinity purification, C2C12 myotubes were transduced with 1×10^{12}, 1×10^{11}, or 1×10^{10} vg of AAV6-CK8e-mFKRP-FLAG (the murine *Fkrp* cDNA with a C-terminal FLAG tag). Cell lysates revealed co-immunoreactivity with the FKRP and FLAG antibodies and provided confirmation of FKRP production by the AAV6-CK8e-FKRP vector (Figure 1A). To maximize protein expression, we searched for potential inhibitory sequences in the *FKRP* UTRs. Sequence analysis suggested that there may be regulatory secondary mRNA structures, so both UTRs were removed from the *Fkrp* cDNA (A6.C8mF). Note, however, that CK8e, which is present in all of these vectors, carries 49 bp from the mouse CKM 5′ UTR and that the poly(A) sequence used was also identical in all vectors (materials and methods). The effects of these modifications were then compared *in vitro* by transducing C2C12 myotubes with vectors either carrying or lacking the *Fkrp* 5′ and 3′ UTRs. Western blot analysis with Ab607 showed a notable increase in FKRP expression upon removal of the UTRs (Figure 1B). It is important to note that the minor bands at 55 kDa correspond to the predicted molecular weight of FKRP, while the larger bands at ~60 kDa are likely the N-glycosylated form of the protein.[50] This vector was then tested *in vivo* via intramuscular injections into the tibialis anterior (TA) of wild-type mice (1×10^{11} vg/muscle).[48] Analysis of injected muscles revealed FKRP expression by western blot as well as mosaic distribution of the protein throughout the injected muscles (Figure 1C). While some FKRP immunostaining colocalized with GIM130 in the Golgi apparatus, much of the exogenous protein was localized diffusely (see also Figure 6), as observed previously by others.[13,16] Wild-type (WT) levels of FKRP expression are beyond the detection limit of our antibody.

To explore potential deleterious effects from high levels of exogenous FKRP expression, we generated a similar vector that expressed the human FKRP (also lacking the *FKRP* 5′ and 3′ UTRs). This CK8e-hFKRP construct was encapsulated into AAV6 (A6.C8hF), AAV9 (A9.C8hF), or AAVMYO1 (AM.C8hF) vectors and tested in various strains of mice via systemic delivery (Figures 1D and 1E).[51] The first cohort, comprised of $FKRP^{P448L}$ mutant mice, was injected with A6.C8hF at doses of 1.5×10^{13} and 1.5×10^{14} vg/kg and analyzed with a variety of tests of muscle strength and exercise performance at different time points (Figure 1E).

A6.C8hF-treated mice show significantly improved grip strength in a dose- and time-dependent manner

Ten-month-old $FKRP^{P448L}$ mutant mice were injected with different doses of A6.C8hF (saline, and 1.5×10^{13} and 1.5×10^{14} vg/kg) and monitored alongside age-matched WT controls. The purpose of using older mice was to address the effect of treatment in older mice with a more advanced phenotype. Forelimb grip strength of age-matched WT, untreated, and treated $FKRP^{P448L}$ mice was measured at 4, 8, 12, and 16 weeks post injection. Absolute forelimb grip strength increased progressively in a dose-dependent manner among treated mice but did not change in WT or untreated $FKRP^{P448L}$ mice (Figure 2A). Compared with untreated $FKRP^{P448L}$ mice, 4 months of treatment with low- and high-dose vector restored strength to approximately 40% and 70%, respectively, of WT levels, although the rate of improvement appeared to level off after 3 months in low-dose mice. Normalizing these data to body weight (Figure 2B) can confound the results, however, because (1) the low-dose group included males and females, whereas the high-dose group included only males, and (2) body weight varied greatly among aged mice and was therefore a poor normalizing factor.[52] In fact, body weight increased modestly in all but the low-dose group (Figure S2), while grip strength increased progressively in all treated $FKRP^{P448L}$ mice. This indicates that changes in grip strength were unlikely to be due to compensatory responses to changes in body weight. To remove the data-biasing effects of sex and age, we then quantified the relative change in strength over time and validated the dose-dependent and temporal increase (Figure 2C).

Hindlimb grip strength measurements are often highly variable until mice become accustomed to the assay. Indeed, grip strength absolute force increased in all groups before stabilizing at 8 weeks (Figure 2D). Absolute force was similar in treated mice regardless of dose and at all time points. However, treated mice were also stronger than untreated mice by this measure, while grip strength in WT and high-dose mice was similar. Normalizing force to body weights eliminated these differences (Figure 2E), although treatment effects were demonstrated for one or both doses at different time points when relative changes were examined (Figure 2F). These results suggest that, despite the innate variability of the assay, treatment with A6.C8hF increased hindlimb grip strength in aged mice.

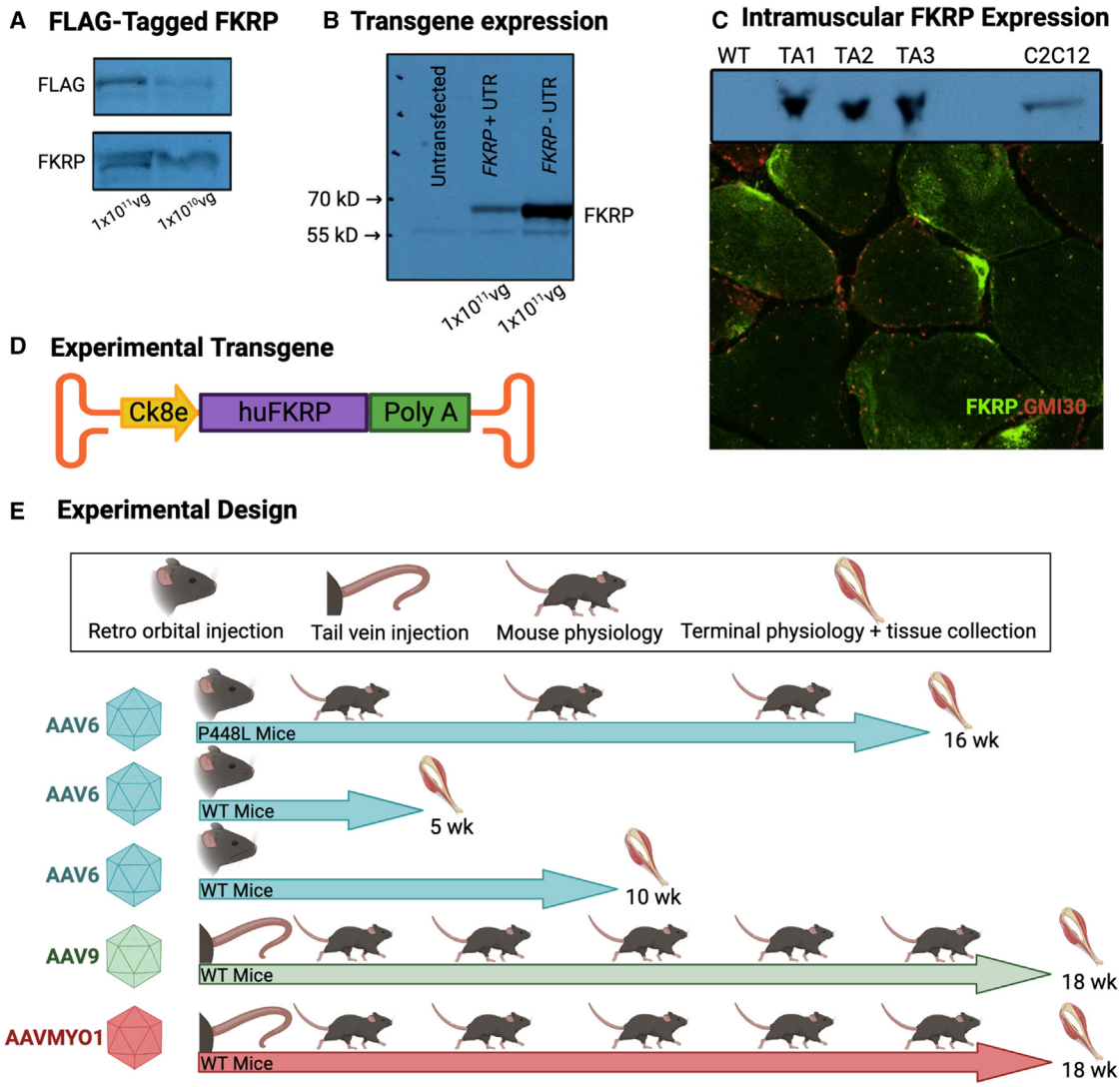

Figure 1. Removal of the *FKRP* 5′- and -3′ UTRs increases FKRP expression

(A)Cell lysates from differentiated C2C12 myotubes transduced with either 1×10^{11} or 1×10^{10} vector genomes (vg) of A6.C8mF-FLAG to verify vector expression of mouse *FKRP* (mFKRP). Labels on the left indicate the antibody target (FKRP, Ab607; FLAG, FLAG-HRP, Sigma F7425). (B) FKRP levels in myotubes transduced with untagged AAV6-Ck8e-mFKRP (+UTR) and AAV6-Ck8e-mFKRP (−UTR). (C) Top: FKRP expression in tibialis anterior (TA) muscles of WT mice injected intramuscularly (i.m.) with 1×10^{11} vg AAV6-Ck8e-mFKRP (−UTR) relative to an untreated WT mouse and C2C12 myotubes transduced with 1×10^{12} vg of the same vector. Bottom: immunostaining of WT TA muscle injected with AAV6-CK8e-mFKRP. FKRP, green. Golgi apparatus, red (GMI30). (D) Schematic of the AAV-CK8e-human FKRP (hFKRP) construct used in these studies. (E) This transgene construct was expressed from vectors pseudotyped with capsids from AAV6 (A6.C8hF), AAV9 (A9.C8hF), or AAVMYO1 (AM.C8hF). WT and $FKRP^{P448L}$ mutant mice were then treated and tested at various time points post injection to identify potential physiological and histological changes. WT, wild-type; P448L, $FKRP^{P448L}$.

Exercise capacity of mice treated with a high dose is improved significantly

The next metrics examined in treated mutant mice included measurements of VO_2max, distance traveled, energy expended, and energy consumption rate (Figures 3A–3H). All of these are measured using a metabolic treadmill and include VO_2max tests to assess changes in maximal O_2 consumption, a measure of exercise capacity and cardiorespiratory function, and several intermittent training sessions meant to exacerbate the dystrophic phenotype.[27–30] Training had a beneficial effect in WT mice and increased VO_2max by almost 10% (Figures 3A and 3B). By contrast, training exacerbates the dystrophic phenotype in untreated $FKRP^{P448L}$ mice because VO_2max was reduced by over 10%. This decline was prevented by A6.C8hF treatment because the slight reduction in VO_2max between tests of treated $FKRP^{P448L}$ mice was not significant. Moreover, the degree of

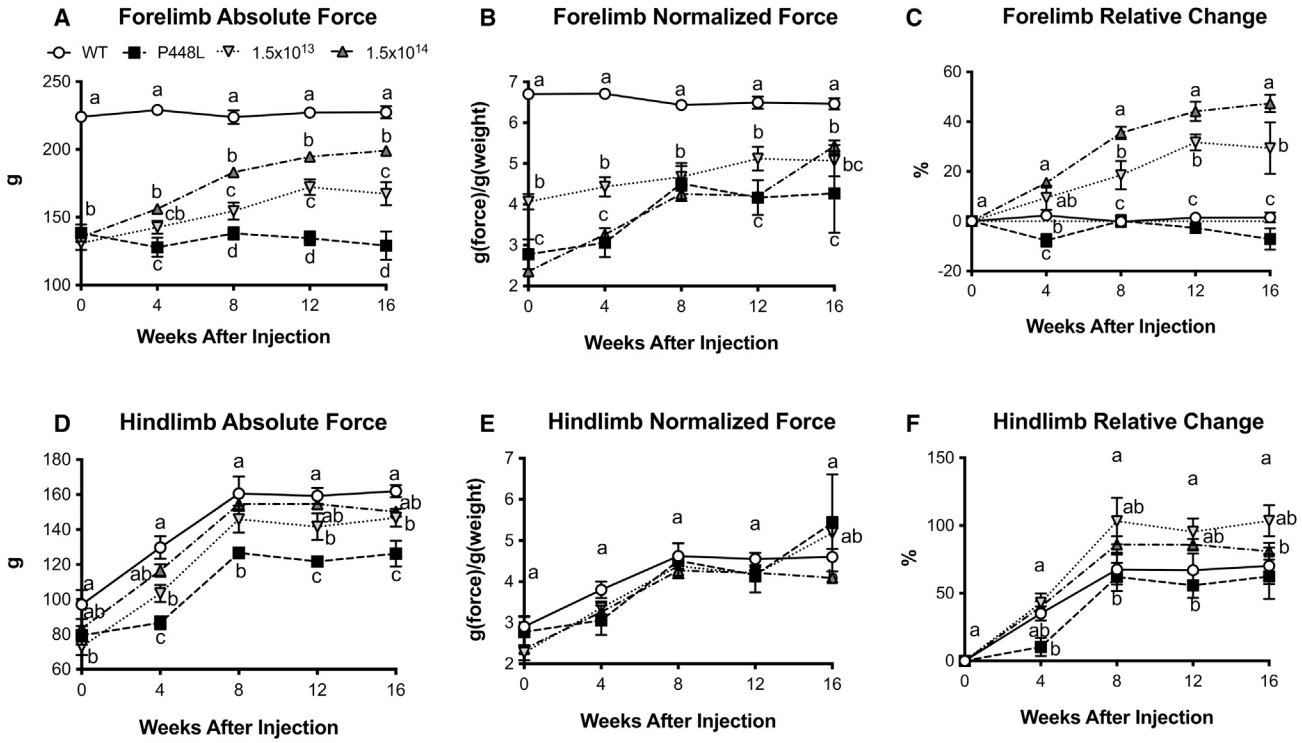

Figure 2. Changes in forelimb and hindlimb grip strength over time

(A–F) Forelimb grip strength (A–C) and hindlimb force (D and E) of WT mice and of mutant mice injected with saline (P448L), 1.5×10^{13}, or 1.5×10^{14} vg/kg A6.C8hF. (A and D) Forelimb grip strength over time. (B and E) Absolute force was normalized to body mass. (C and F) Percent change from absolute force measurements at baseline. All mice were 10 months old at baseline. Significant differences between treatment groups at a given time point are indicated by different letters, whereas shared letters indicate no difference. P448L, untreated (mean +/- S.E.M., n = 4–5).

relative change between tests was highly significant among all three groups (Figure 3B), clearly indicating the effect of impact training and treatment. Changes in running distance and energy rate (Figures 3D, 3F, and 3H) reflected a similar relationship because impact training improved, impaired, or had no effect on WT mice, untreated FKRP^{P448L}, and treated FKRP^{P448L} mice, respectively. These results collectively suggest that, although high-dose treatment with A6.C8hF may not restore exercise capacity and cardiorespiratory function to WT levels, it prevents the deleterious effects of impact training and improves striated muscle functional efficiency.

Both FKRP^{P448L} groups of mice ran shorter distances in the initial tests while expending similar calories (Figures 3C and 3E). Although this resulted in higher energy consumption rates, these differences were not significantly different from WT mice (Figure 3G). The protective effect on exercise-induced impact was also reflected in energy consumption rates. In fact, all three groups were significantly different from one another in the final test, with untreated FKRP^{P448L} mice having the lowest VO_2max and highest energy consumption rate (Figures 3A and 3G). Treated FKRP^{P448L} mice displayed values closer to those of WT animals. These data indicate that FKRP^{P448L} mice work harder to run shorter distances while consuming less oxygen. By contrast, treatment with A6.C8hF partially restored these metrics and, thus, exercise capacity.

High-dose A6.C8hF partly ameliorates the dystrophic respiratory pattern and endurance exercise capacity in FKRP^{P448L} mice

Several pathological markers for assessing exercise impact training have been developed for dystrophic mice.[27–30] In addition to histological metrics, these include several exercise-induced markers in FKRP^{P448L} mice, such as variability in respiration (VO_2cv), the respiratory exchange ratio (RER, VCO_2/VO_2), energy expended, and the accumulation of motivational shocks.[29,30] In 4 of the 6 training sessions, the VO_2cv values for untreated FKRP^{P448L} mice were higher than those for WT mice, while the treated FKRP^{P448L} animals displayed values that were either significantly lower than those of the untreated mice or not different from those of WT mice (Figure 4A). A similar pattern was observed when comparing the overall differences between groups, which were highly significant, and when assessing differences in maximal RER values (Figure 4B).

No differences between groups were noted when assessing energy expenditure (Figure 4C), although, by contrast, many differences were noted in the accumulation of motivational shocks (Figure 4D).

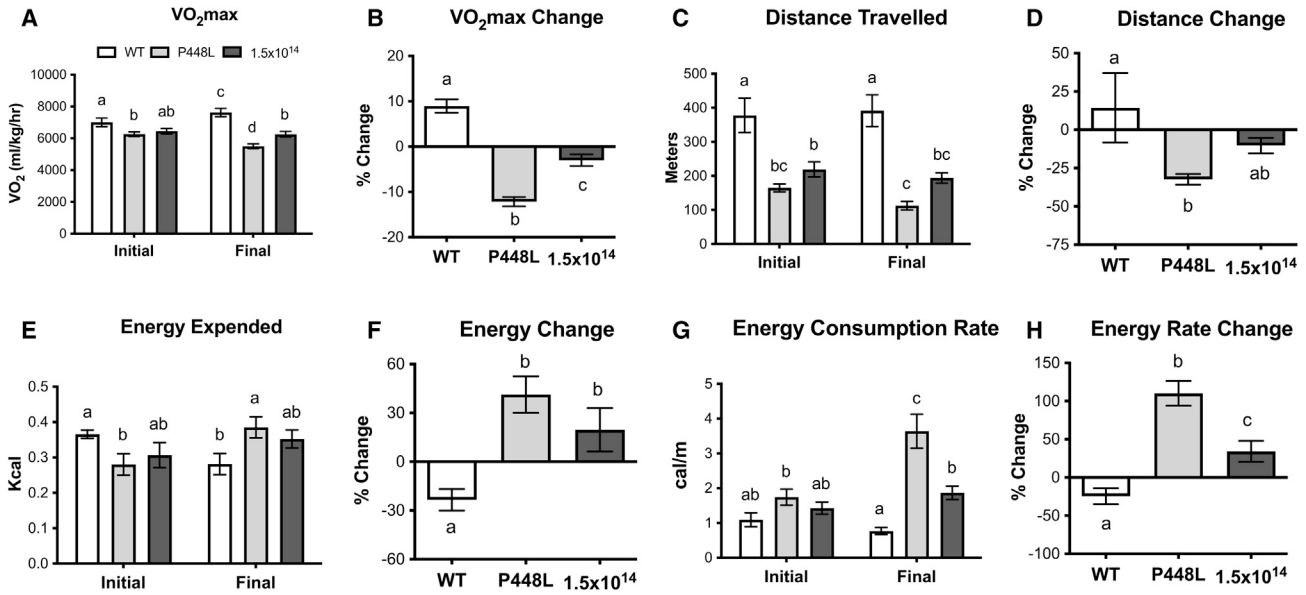

Figure 3. Energetics of exercise performance

WT and mutant mice were injected with saline (WT and P448L, respectively), the latter also with 1.5×10^{14} vg/kg. After 12 weeks, VO_2max tests were performed (initial) on all mice, which then trained twice a week for 4 weeks followed by a final VO_2max test. (A and B) VO_2max values for each time point and the change from initial to final. (C and D) Distance traveled before mice fatigued, failing to re-engage the treadmill, and the change from initial to final. (E–H) The total energy expended during tests was calculated using indirect calorimetry (E and F) and normalized to the total distance traveled for each mouse to quantify the energy consumption rate (G and H). Significant differences are represented by different letters, and shared letters indicate no difference. P448L, untreated (mean +/- S.E.M., n = 5–6).

In fact, the number of shocks received by untreated $FKRP^{P448L}$ mice was approximately 6-fold higher than for the WT in all training sessions. However, treating $FKRP^{P448L}$ mice with A6.C8hF significantly reduced these numbers by the third session. Although levels were never restored to normal WT levels, they remained significantly below those of untreated $FKRP^{P448L}$ mice. Inordinate shock accumulation is a striking feature of $FKRP^{P448L}$ mice[30] that could be related to a previously documented Trendelenburg-like gait abnormality.[30] Thus, these results suggest that A6.C8hF may partly restore many aspects of muscle function and exercise performance that may even influence gait.

Mutant mice treated with A6.C8hF have decreased muscle degeneration, improved fiber size distribution, and decreased CK levels

After the final VO_2max test, all mice were sacrificed and different muscles were collected. Compared with untreated $FKRP^{P448L}$ mice, treated $FKRP^{P448L}$ mice had larger skeletal muscle myofiber sizes (Figures 5A–5C), fewer centrally nucleated myofibers, and fewer total centrally located nuclei (Figures 5D and 5E), hallmarks of prior rounds of muscle necrosis and regeneration. This was generally true for all muscles tested, although the diaphragm displayed non-significant differences between treated and untreated mice. The most dramatic response to treatment was the nearly 5-fold reduction in serum CK levels in treated vs. untreated mice (Figure 5F). These data together suggest that A6.C8hF reduces exercise-induced muscle damage that activates cycles of necrosis and regeneration that lead to skeletal muscle atrophy.

AAV injection leads to non-uniform FKRP expression in WT and treated $FKRP^{P448L}$ mice

We performed immunofluorescence (IF) analysis of FKRP localization in muscle cryosections using Ab607. We first examined the TA and heart from mutant mice treated with 1.5×10^{14} vg/kg A6.C8hF at 10 weeks post injection (Figure 6A). At this time point, FKRP was widely expressed in both muscle types, albeit in a mosaic pattern, consistent with previously reported results.[10] $FKRP^{P448L}$ mice were then administered higher doses of A68hF (1.5×10^{13} and 1.5×10^{14} vg/kg) that increased grip strength and exercise capacity (Figures 2, 3, 4, and 5), which is suggestive of sufficient FKRP expression to partially rescue the disease phenotype (Figures 2, 3, 4, and 5). While endogenous FKRP was difficult to detect in untreated mice, more FKRP IF was observed in heart tissue from exercised vs. sedentary mice (Figure 6B and data not shown). In contrast, treated (sedentary) mice displayed robust expression of FKRP in a dose-dependent manner. The effect of exercise is intriguing; while it has been shown previously that $FKRP^{P448L}$ mutations can lead to a cardiac phenotype,[15] to our knowledge, exercise-induced FKRP expression has not been studied previously.

WT animals treated with AAV-FKRP vectors displayed normal muscle physiology

To explore multiple approaches for delivering FKRP to skeletal muscles and simultaneously monitor for toxic effects, we performed additional assays in WT mice injected with vectors made with AAV6, AAV9, or AAVMYO1 capsids. These studies also provided a way

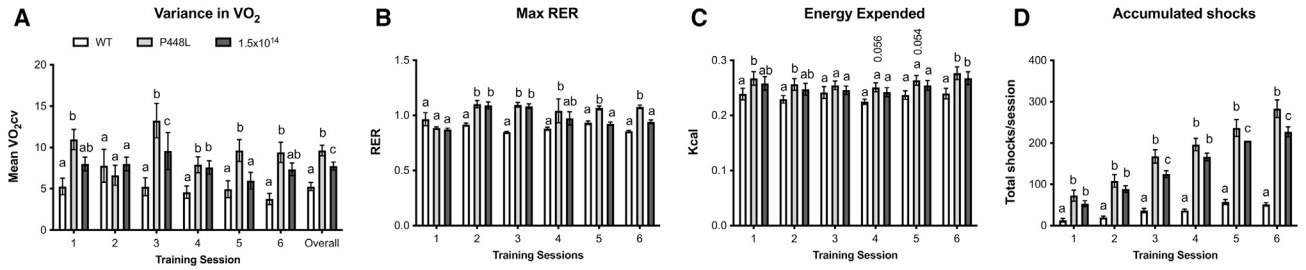

Figure 4. The effects of exercise impact training in the high-dose experiment

After an initial VO_2max test, WT mice and $FKRP^{P448L}$ mice were injected with saline (P448L) or 1.5×10^{14} vg/kg A6.C8hF and then trained on respiratory treadmills twice a week for 6 sessions. Mice ran with submaximal effort at the same speed and for the same time while respiratory gas exchange was continuously monitored. (A) The fluctuating breathing pattern common to dystrophic mice was quantified by calculating the VO_2 coefficient of variation (VO_2cv). (B) Differences in maximum respiratory exchange ratio (RER) with each session. (C) Total energy expended during each session was calculated using indirect calorimetry. (D) Electrical shocks were used to encourage mice to re-engage the treadmill, and their quantification reflects this ability. In each panel, the numbers on the x axis represent specific training sessions, and different letters above the histograms are used to signify significant differences between any two means ($p < 0.05$ unless otherwise indicated); shared letters indicate no difference. P448L, untreated (mean +/- S.E.M., n = 5–6).

to examine the effects of exogenous FKRP in muscle already expressing normal levels of the enzyme. In particular, one previous report suggested that overexpression of FKRP could impair the formation of a functional DGC.[13] Our studies used AAV6, as above, but also 2 additional vector types. Gene therapy agents featuring AAV9 capsids are commonly used in clinical trials for different neuromuscular disorders,[30] while the recently developed AAVMYO1 has been reported to provide significantly enhanced muscle transduction.[34] By using AAV vectors pseudotyped with multiple capsids, including a potent myotropic capsid (AAVMYO1), our results were not limited to the effects of a single type of AAV capsid.

The first study consisted of WT mice injected with A6.C8hF at doses of 4×10^{13}, 2×10^{14}, or 4×10^{14} vg/kg to determine whether this vector caused an increase in susceptibility of muscles to contraction-induced injury. These high doses were used in this preliminary safety assessment because doses at or exceeding 1×10^{14} vg/kg have often led to serious adverse events in patients with various neuromuscular disorders.[30–32,53,54] This is important because a high-dose AAV-mediated FKRP therapeutic agent plus endogenous FKRP provides the ability to maximize potential expression. Some of these mice underwent gastrocnemius muscle physiology assays 5 weeks later, and others were tested at 10 weeks. However, we did not observe any deleterious impact on mechanical properties at these doses (Figure S1).

Finally, the AAV9 and AAVMYO1 vectors were injected into WT mice at doses of 6.4×10^{12}, 2×10^{13}, and 6.4×10^{13} vg/kg. The latter two cohorts of mice were analyzed for a variety of properties at 4, 6, 8, 10, 12, and 14 weeks post injection to evaluate effects on muscle physiology (Figure 7). At 6, 10, and 14 weeks post injection, fatigue assays were performed where mice ran on a treadmill at a speed of 10 m/s with 1 m/s/minute increases (Figures 7A–7C). No differences were detected between groups at each time point. Moreover, the absence of differences in relative change within and between groups similarly demonstrates an absence of detrimental effects on running fitness and fatiguability following vector delivery. We also examined forelimb grip strength between 4, 8, and 12 weeks post injection. Although mice treated with AAV9 displayed reduced force over time, there were no differences between groups at any time point. In fact, all the mice (treated and untreated) experienced a decrease in strength between 10 and 14 weeks post injection, which typically occurs when mice habituate to the grip strength assay.

Another commonly used assay in mouse muscle analysis is the ankle plantar flexion assay, where ankle torque over 20 eccentric contractions is quantified using a high but physiologically relevant stimulation frequency that elicits a maximal response. The assay is designed to assess force generation in addition to fatigue caused by repeated eccentric contractions. At all time points, torque declined to 50% of starting baseline measurements, consistent with contraction-induced fatigue (Figures 7G and 7H). However, no differences were detected between any of the three groups at any time point. This includes potential differences in torque at a given contraction as well as the relative change from baseline. These results further suggest that A9.C8hF and AM.C8hF treatments at a dose of 6.4×10^{13} vg/kg did not compromise muscle force generation or enhance fatiguability.

To identify potential adverse consequences of exogenous FKRP expression in cardiac and diaphragm muscles, we used ultrasound imaging to measure cardiac ejection fraction and fractional shortening as well as diaphragm displacement. Ejection fraction measures the percentage of blood leaving the left ventricle, while fractional shortening is a measure of the heart's contractility; both are common indicators of cardiac function. Diaphragm displacement is an indicator of respiratory function. No differences were detected between untreated and treated groups, likely because of the small sample size (n = 3–4); however, more data may highlight the increased injection fraction of AM.C8hF over A9.C8hF and untreated mice (Figures 8A–8C). At the experimental endpoint (18 weeks post injection), skeletal muscle function was further assessed using a contraction-induced injury protocol on TA and diaphragm muscles. Here, muscles were stretched by an additional 5% between contractions to measure specific force

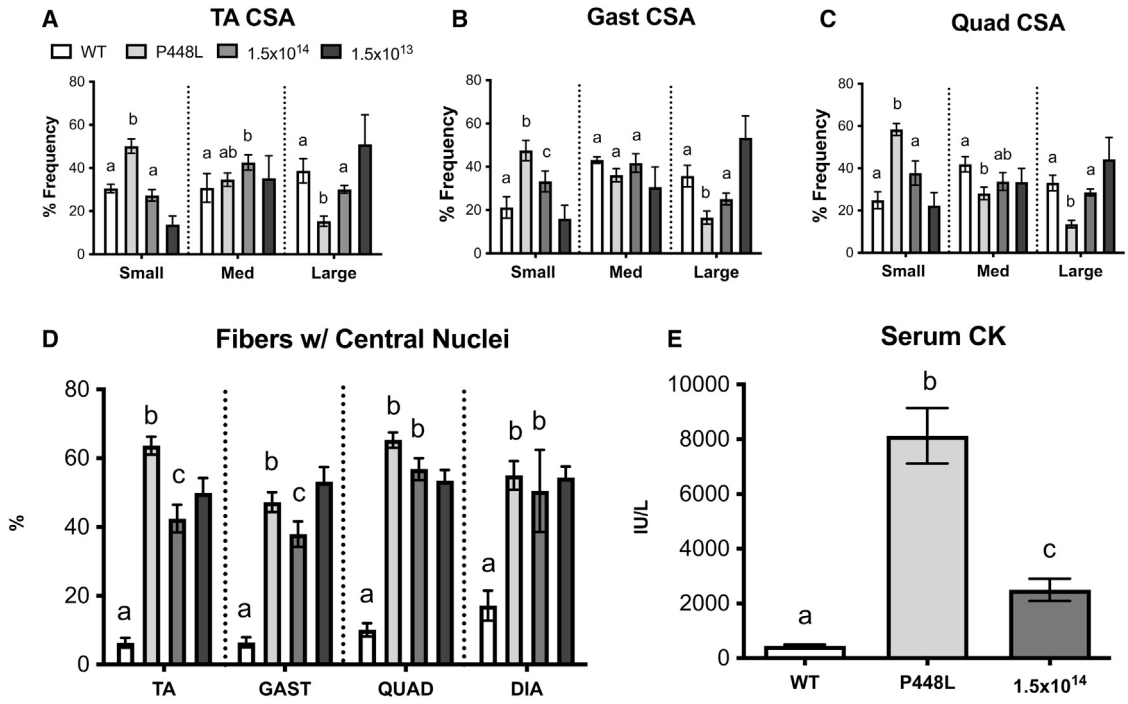

Figure 5. Morphological changes induced by *FKRP* delivery

10-month-old FKRP^{P448L} mice were treated systemically with 1.5 × 10^{14} vg/kg A6.C8hF and analyzed 4 months later. (A–C) Fiber cross-sectional area (CSA) of the indicated muscles parsed by fiber size groups: less than 3,000 μm, small; 3,001–7,000 μm, medium; more than 7,000 μm, large. (D and E) Fiber and nucleus counts per field in different skeletal muscles (GAST, gastrocnemius; QUAD, quadriceps; DIA, diaphragm). (F) Serum CK levels in treated mice. Significant differences are represented by different letters, and shared letter indicates no difference. P448L, untreated (mean +/- S.E.M., n = 3–5).

development and to examine the effects of contraction-induced injury on force. As with the other functional assays, no differences were detected between treated and untreated groups (Figures 8D and 8E). These data complement those from previous tests and together reveal no adverse consequences from exogenous FKRP overexpression in skeletal or cardiac muscles using the assays shown (Figures 7 and 8).

DISCUSSION

This study demonstrated that A6.C8hF (carrying the *FKRP* cDNA lacking UTRs) ameliorated pathophysiology associated with the dystrophic phenotype in aged FKRP^{P448L} mice. Moreover, it also significantly minimized exercise-induced impacts on skeletal muscle structure and function, with a treatment benefit proportional to the dose of A6.C8hF administered and without obvious safety side effects. One focus of our investigation was to develop a transgene with high expression levels in striated muscles. Use of such a transgene can enable studies of safety while facilitating therapeutic expression levels at lower vector doses. It should be noted that safety and toxicity concerns have been growing in the field, with adverse events from either the vector or transgene being observed in a variety of high-dose, neuromuscular disease AAV trials.[55,56]

RGQs are known to regulate gene expression and have been targeted as a strategy to ameliorate or worsen genetic disease pathologies.[40,57] We discovered that complete removal of the 5′ and 3′ UTRs led to increased gene expression (Figure 1). These data suggest the presence of inhibitory regulatory sequences within the UTRs of *FKRP*, which could provide a potential target for fine-tuning gene expression. The occurrence of toxicity associated with gene overexpression has sometimes been resolved by targeting UTRs,[37,58] which continue to be evolved for even more influence over protein production.[59]

Differences in the design of the various experiments in our study prevent direct comparisons of many metrics. Nevertheless, we can compare several differences between treated and untreated FKRP^{P448L} mice within individual experiments to gauge the relative sensitivity to gene delivery. Overall, treatment had a clear beneficial effect, and no adverse events were observed at any doses in either WT or mutant mice. It should be noted that, while improvement occurred in a dose-dependent manner, none of the functional metrics were restored to WT levels using the doses tested. This was not unexpected because FKRP mutations in animal models and patients lead to a degenerative disease that progressively develops and worsens with age,[60–62] compounding challenges to drug efficacy. Higher doses or ancillary treatments to enhance muscle mass and strength may be needed when degeneration is advanced.

Other FKRP gene therapy studies generally used young FKRP^{P448L} mice and reported many significant improvements in the structure and function of skeletal and cardiac muscle.[11,15] Only one study

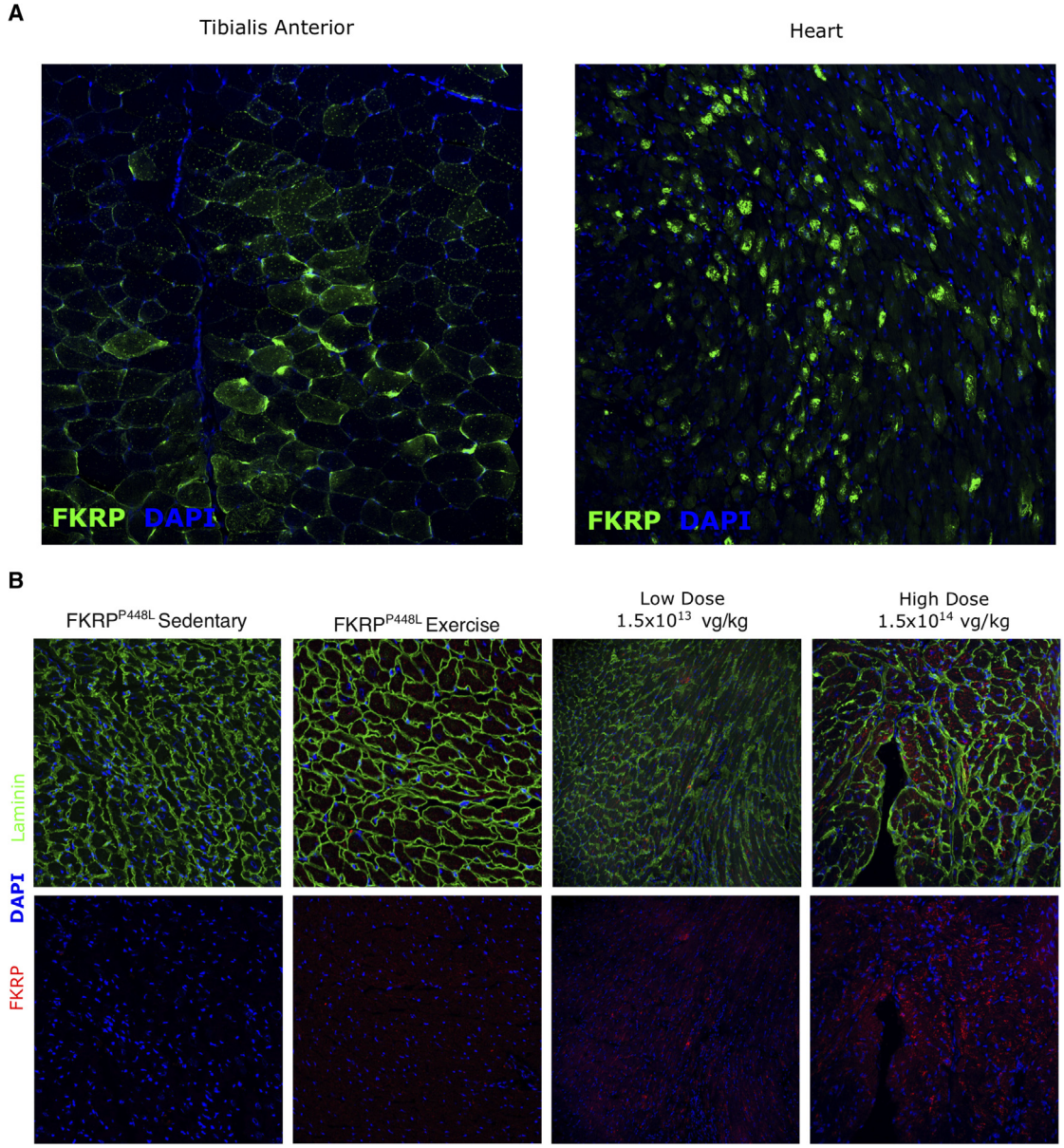

Figure 6. staining reveals mosaic expression of exogenous FKRP

(A) TA and heart muscles from FKRP^{P448L} mice treated with 1.5 × 10^{14} vg/kg of A6.C8hF were isolated 10 weeks post injection, and cryosections were prepared and analyzed. Shown is immunostaining for FKRP (green); DAPI staining is shown in blue. (B) Cryosections from hearts of FKRP^{P448L} mutant mice, comparing FKRP expression in untreated mice following no exercise (sedentary, leftmost panels), and in untreated mice (active) and treated mice that were exercised, all at 16 weeks post injection. Treated mice received an intravenous injection with a high (1.5 × 10^{14} vg/kg) or low (1.5 × 10^{13} vg/kg) dose of A6.C8hF and were exercised. Shown is immunostaining for FKRP (red) and laminin (green); DAPI staining is shown in blue.

used an exercise paradigm to assess therapeutic efficacy in FKRP^{P448L} mice.[18] While that study did not incorporate respiratory measures or impact training, a variety of age groups was tested, including aged 39-week-old mice treated for 12 weeks. Those treated FKRP^{P448L} mice displayed increased fatigue resistance, running time, and maximal speed in all age groups, although the differences reported were not statistically significant. Regardless, that trend is consistent with the current study and further suggests that systemic FKRP gene therapy can enhance exercise capacity even in aged FKRP^{P448L} mice.

Demonstrating that our therapeutic agent can improve exercise capacity is especially meaningful because the metrics measured are largely dependent on cardiac rather than skeletal muscle function.

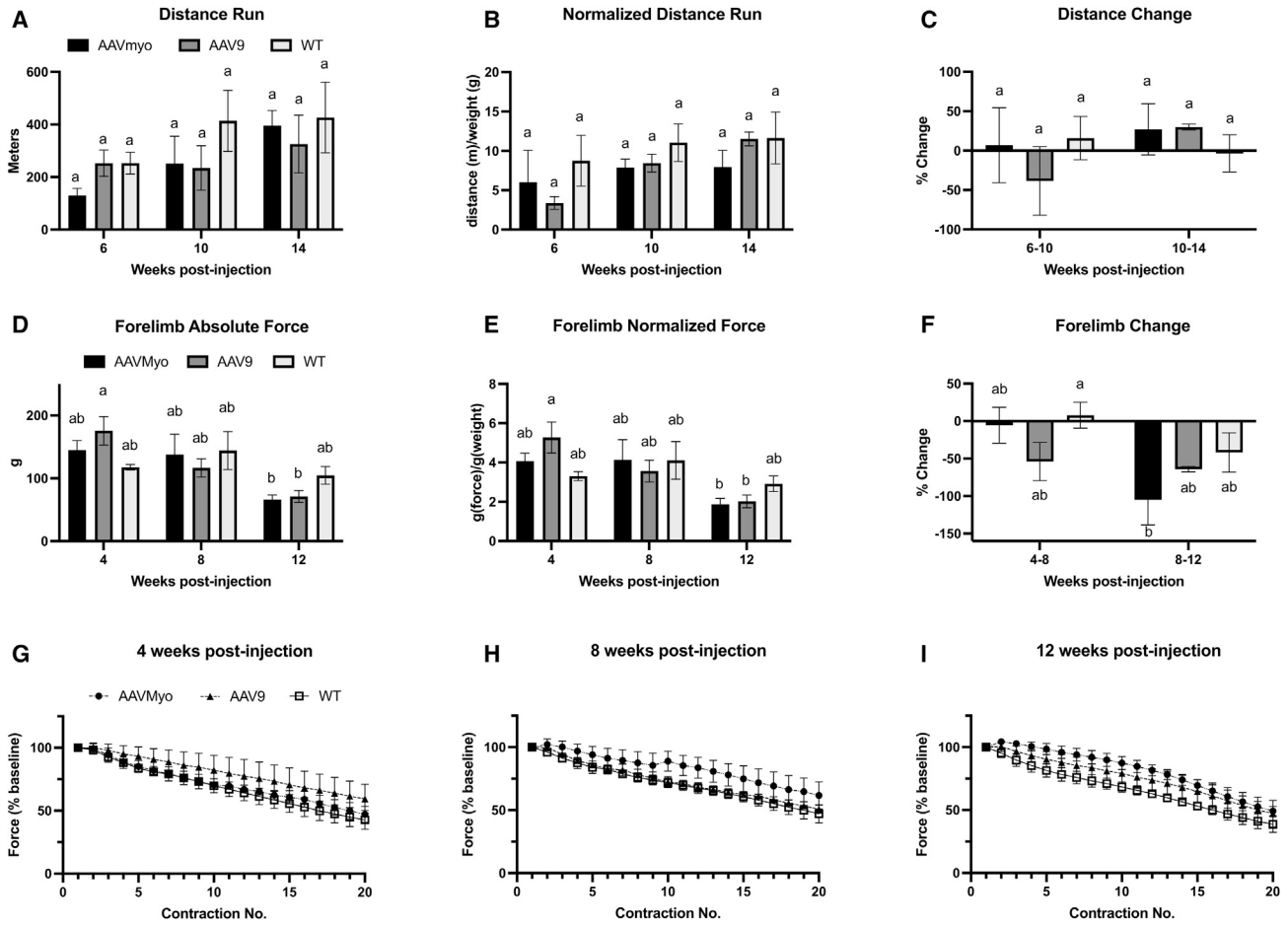

Figure 7. Whole-body and isolated limb physiology of WT mice treated with AAV-hFKRP

(A) Distance run on a treadmill by mice injected with either saline (WT) or 6.4×10^{13} vg/kg of A9.C8hF or AM.C8hF. (B) Distance run normalized to mouse weight. (C) Percent distance changed relative to previous absolute distance measured. (D) Forelimb grip strength. (E) Forelimb grip strength normalized to mouse weight. (F) Percent forelimb grip strength changed relative to absolute grip strength. (G–I) Repeated cycles of plantar flexion eccentric contraction-induced injury (20×) in the right hindlimb of mice at 4, 8, and 12 weeks post injection, measured by hindlimb torque. The limb was stimulated with 10 mA at a frequency of 100 Hz for 0.4 s with a 9-s rest interval between contractions. Significant differences are represented by different letters, and shared letter indicate no difference. WT, untreated (mean +/- S.E.M., n = 3–4).

Thus, the improved performance in VO_2max tests suggests that cardiac function is specifically enhanced (Figure 3). These results are complemented by others[16] that demonstrate that *FKRP* delivery to mutant mice can improve some aspects of cardiac contractility in stress tests. Left ventricle dysfunction has been described in FKRP^{P448L} mice[30] and often occurs in human subjects with LGMDR9. Moreover, cardiac and respiratory impairment directly contribute to mortality in many individuals with different FKRP mutations and are predictors of long-term survival. It is not unreasonable, therefore, to presume that systemic FKRP gene therapy could ameliorate the primary cause of mortality in LGMDR9 patients.

Our AAV vector also protected FKRP^{P448L} mice from many degenerative effects of impact training. This included changes to muscle structure, serum CK levels, and exercise capacity (Figure 5). Impact training is known to accelerate and exacerbate muscle degeneration in dystrophic mice and is considered an advanced stressor.[63] The fact that A6.C8hF protected aged FKRP^{P448L} mice from impact training is significant and suggests that treatment overcame the accumulated effects of age, as indicated by improved functional metrics before initiating training as well as the damage from repeated exercise, as indicated by the improved functional metrics during the training sessions and by the histological metrics. Differences in cross-sectional area and central nucleation between treated and untreated FKRP^{P448L} mice were more apparent in TA and quadriceps muscles than in the gastrocnemius or diaphragm. The former two muscles have a higher type II fiber composition than the latter mixed-fiber type muscles. This result suggests that FKRP gene therapy may be especially effective in stabilizing predominantly fast-twitch muscles that are more affected in different muscular dystrophies.[64,65]

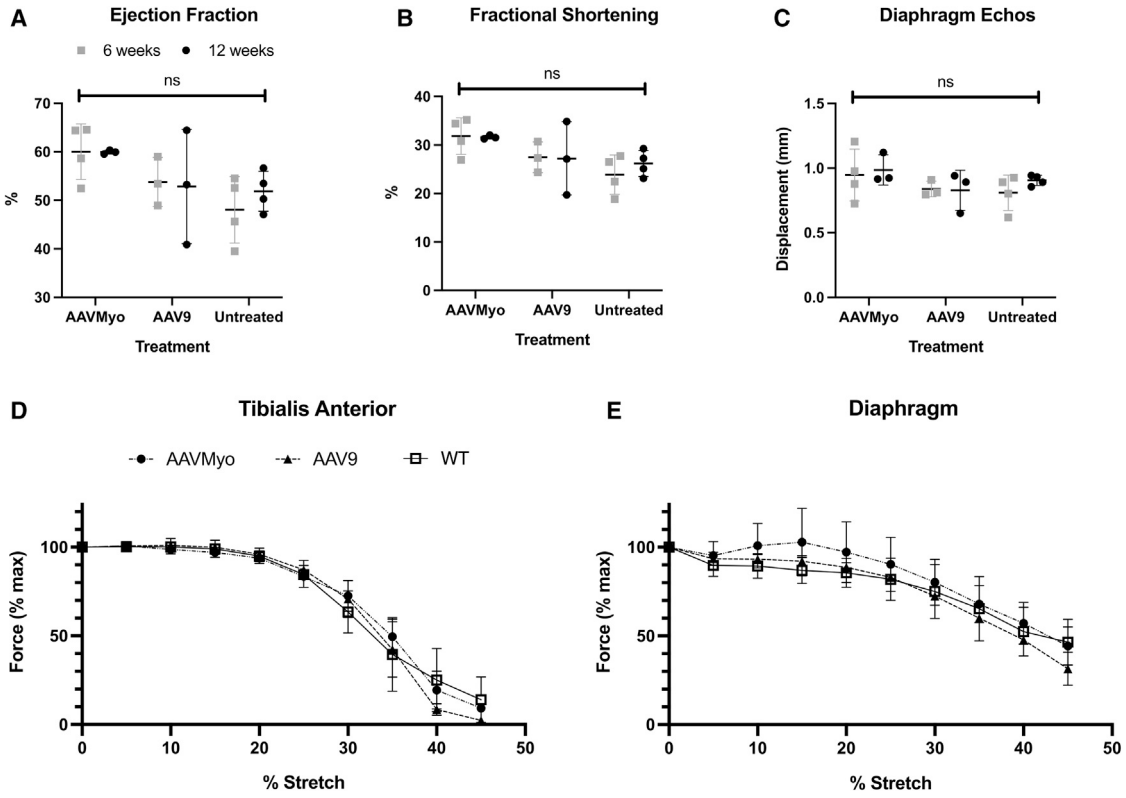

Figure 8. Cardiac hemodynamics and skeletal muscle mechanics following AAV delivery to WT mice

Mice were left untreated or injected with 6.4×10^{13} vg/kg A9.C8hF or AM.C8hF. (A–C) Ultrasound imaging of heart and diaphragm function at 6 and 12 weeks post injection. (D and E) Force:length relationship of TA and diaphragm muscles from same mice at 18 weeks post injection. Muscles are stretched end to end, and optimal length is determined at maximum isomeric twitch force (materials and methods). No differences were detected in these data. WT, untreated (mean +/- S.E.M., n = 3–4).

Safety assessment with exogenous FKRP expression

While studies here and by others show improved phenotypic outcome from AAV-FKRP delivery, we also explored the effects in WT mice to monitor potential adverse events from exogenous FKRP expression above normal muscle expression. These exogenous expression levels were augmented using a strong, muscle-specific regulatory cassette (CK8e), removal of UTRs from the *FKRP* cDNA, and the of myotropic AAV capsids, especially AAVMYO1. The AAVMYO1 capsid in particular is one of a new class of potent muscle-targeting capsids and may allow lower doses to be used in clinical trials.[33–35] Three doses of 4×10^{13}, 2×10^{14}, and 4×10^{14} vg/kg of A6.C8hF indicated that treated WT mice continued to gain strength, did not fatigue more rapidly, and showed no detrimental effects on mechanical properties (Figure S1). We also performed a longer study with WT mice left untreated or injected with A9.C8hF and AM.C8hF. These groups of mice showed no significant differences in distance run, forelimb grip strength, or TA, diaphragm muscle, or hindlimb eccentric contraction-induced fatigue over time, nor were these measurements significantly different between groups (Figure 7). In these studies, treated and untreated mice also showed no change in ejection fraction, fractional shortening, or diaphragm displacement over time (Figure 8). Overall, our data support the safety of A6.Ch8F, A9.C8hF, and AM.Ch8F as gene therapies for LGMDR9 because our assays show that none of these treatments led to adverse effects on WT mouse physiology. These results demonstrate that expression from the vectors used was not deleterious to muscle function and was able to ameliorate disease pathology in mutant mice.

Conclusions and future directions

Our studies further support the feasibility of gene therapy for disorders resulting from FKRP mutations. Like previous studies, we observed an overall significant amelioration of disease phenotype in adult $FKRP^{P448L}$ mice.[11,12,18] Further, we did not observe any obvious detrimental effects from expression of FKRP using a variety of AAV vectors at different doses in WT mice. A potential G-quadruplex in the 5′ UTR may serve to limit expression, although we did not dissect individual bases in the 5′ or 3′ UTRs of the *FKRP* mRNA that mediate this effect. The difficulty encountered by many labs in detecting endogenous *FKRP* expression suggests that extremely low levels of the enzyme are all that is needed for normal glycosylation of α-DG. It is possible that inhibitory UTR sequences may serve a role in limiting overexpression during normal muscle activity, although further studies would be needed to clarify this issue. Importantly, the safety of this therapeutic agent observed in our studies supports

continued advancement of methods for gene therapy to treat patients carrying mutations in the *FKRP* gene.

MATERIALS AND METHODS

Animals

All animal experiments were approved by the Institutional Animal Care and Use Committee of the University of Washington or Washington State University. For the $FKRP^{P448L}$ mutant experiments, mice were obtained from the Lu lab[15] and maintained by the Rodgers lab at Washington State University. The studies using $FKRP^{P448L}$ mice began when the mice were 10 months old. The other mouse studies were performed in C57BL6 WT male mice aged 6–35 weeks at age of injection.

Plasmid construction and vector production

The coding region of mouse *Fkrp* was PCR amplified (forward primer, 5′ TTGTTAACATGCGGCTCACCC-3′; reverse primer, 5′ TACCGGTTCAACCGCCTGTC-3′) from mouse muscle cDNA. The resulting DNA fragment was digested with *HpaI* and *AgeI* and ligated into an AAV backbone vector containing a muscle-specific CK8e promoter and synthetic poly(A) tail as described previously.[41] Briefly, a custom AAV transfer plasmid containing the previously described muscle-specific CK8e regulator cassette,[41–47] a 1,482-bp cDNA expression construct for native mouse *Fkrp* mRNA (NCBI CCDS20853.1), a synthetic poly(A) signal,[41] and flanking AAV serotype 2 inverted terminal repeats was constructed using standard recombinant methodology. The resulting plasmid, pAAV-CK8e-FKRP, was then used to co-transfect HEK293 cells along with the pDGM6 helper plasmid to generate the AAV6 vector as previously described.[66] For the AAV9 (pA9.C8hF) and AAVMYO1 (AM.C8hF) vectors, the human *FKRP* cDNA was PCR amplified and cloned into pAAV-Ck8e-FKRP in place of the mouse cDNA. These latter vector preparations were produced and purified by Forge Biologics (Grove City, OH, USA).

Antibody production and purification

Rabbit polyclonal antiserum was generated against a peptide near the C terminus of the FKRP sequence that was identical in the mouse and human proteins (as a fusion with KLH: KLH-C-APNNYRRFLELKFGPGVIENPQYPNP) by Covance (Denver, PA, USA). Affinity purification was performed using a maltose-binding protein fusion of the antigenic peptide on MBPTrap HP columns (GE Healthcare) and coupled to Ultralink Biosupport polyacrylamide resin (Thermo Scientific) according to the manufacturer's instructions. The FKRP-C antibody (named Ab607) was affinity purified by HPLC through MBP-FKRP coupled beads and stored in BSA and NaN_3.

Cell culture

Mouse C2C12 cells were plated at ∼80% confluence on gelatin-coated 6-well plates with standard growth medium (DMEM, 20% fetal bovine serum [FBS], and 1% penicillin-streptomycin [P/S]) overnight, then washed three times with 1× saline G prior to infection with rAAV6-CK8-mFKRP. Vectors were diluted to the desired concentrations in differentiation medium (DMEM, 2% HS, and 1% P/S). Cells in each well were incubated with 0.5 mL of diluted virus at 37°C for ∼2 h, brought to a final volume of 2 mL with differentiation medium, and incubated overnight prior to refeeding with fresh differentiation medium. Western blot analysis was performed on day 3 post differentiation to determine FKRP expression.

Gene delivery

Mice were randomly assigned to groups prior to treatment. They were then anesthetized by an intraperitoneal injection of 0.25 mg/g 2,2,2-tribromoethanol or isoflurane and subsequently injected retro-orbitally (RO) (150 μL at doses of 1.5×10^{13}, 4×10^{13}, 1.5×10^{14}, 2×10^{14}, or 4×10^{14} vg/kg), intramuscularly (30 μL at doses of 1×10^{10} and 1×10^{11} vg), or intravenously via the tail vein (150 μL at a dose of 6.4×10^{13} vg/kg).

Western blot analysis

Frozen muscles were ground to fine powder and proteins extracted in 1× Laemmli buffer (62.5 mM Tris-HCl [pH 6.8], 2% SDS, 10% glycerol, and protease inhibitor [Roche]). Lysates were centrifuged at 10,000 × *g* for 10 min at 4°C, and supernatants were transferred to fresh tubes. Total protein concentration was determined by BCA assay (Pierce). Prior to loading, 50 mM DTT and 0.01% bromophenol blue were added to samples and heated at 94°C for 4 min. For each sample, 20 μg of total protein was separated on 4%–12% SDS-PAGE (Life Technologies), transferred to polyvinylidene fluoride (PVDF) membranes (GE Healthcare), and blocked (5% skim milk, 1× PBS and 0.1% Tween 20) for 1 h at room temperature. Blots were probed with Ab607 (1:2,000) overnight at 4°C, washed in 1× PBS-Tween, incubated with horseradish peroxidase (HRP) rabbit secondary antibody (1:20,000, Pierce), and developed with enhanced chemiluminescence (ECL) reagents (GE Healthcare).

Physiology

Grip strength

Fore- and hindlimb grip strength of mutant mice and controls was measured using a grip strength meter (Columbus Instruments, Columbus, OH, USA). Forelimb assays used the T bar or the wire mesh attachment, while hindlimb assays used only the wire mesh attachment. For each mouse, measurements were replicated 5 times in each session with at least 1 min rest between measurements because this ensures accuracy, reduces variability, and prevents habituation. Means were then calculated for each mouse at each time point, and these values were then used to create means for each group.

Treadmill acclimation and forced exercise protocol design for mutant mice

We utilized a four-lane Oxymax FAST modular treadmill system equipped with shock monitors (Columbus Instruments) to measure exercise capacity and respiration during forced exercise of the mutant mice. The motivational shock units were set at level 2.5, providing 0.65 mA of constant current for 200 ms at a frequency of 1 Hz, and fresh air was pumped into the treadmill chamber at a rate of 0.6 L/min. Acclimation runs were performed by placing mice on stationary treadmills

for 5 min with the shock unit engaged. The treadmill was then set at a speed of 5 m/min, and mice walked for 5 additional minutes. This process was repeated for three consecutive days or until mice received 3 or fewer shocks while walking. Exercise training is an excellent means to assess disease pathophysiology in dystrophic mice and is often used to exacerbate the dystrophic phenotype.[27–30] Mutant mice injected with the high dose were trained on a treadmill to assess exercise-induced impact on the dystrophic phenotype. Initial VO_2max tests were performed on high-dose mice 3 months post injection and were followed by 6 training sessions over a month, 2 sessions/week, and then a final VO_2max test. This protocol was recently customized for $FKRP^{P448L}$ mice[30] and is similar to a protocol we established previously for mdx mice.[29] Briefly, VO_2max tests began with mice acclimating on a stationary treadmill for 5 min. Treadmill speed then increased at rates of 5, 9, 12, and 15 m/min for 5 min at each speed. The speed was then increased 1.8 m/min every 2 min until mice reached exhaustion, as indicated by their failure to re-engage the treadmill for 10 s, after which the shock units were turned off. A VO_2max value for each mouse was identified by a rapid increase in the RER approaching 1.1 in combination with a peak VO_2 (mL/kg/h), and caloric expenditure was calculated using indirect calorimetry as described previously.[29,67,68] Mice trained on a 0° incline that began with a 5-min stationary phase followed by 2 min at 5 m/min, 8 min at 8 m/min, and finally 25 min at 12 m/min.

Muscle histology and serum CK assays

TA, gastrocnemius, quadriceps, and diaphragm skeletal muscles as well as the heart were collected from mutant mice and flash frozen in −140°C isopentane. Skeletal muscles were then sectioned at 10 μm on a cryostat, fixed for 10 min in 4% paraformaldehyde, and stained using hematoxylin and eosin. Each slide contained 8–10 sections based on muscle size, and stained slides were imaged using a Nikon Eclipse Ti and a 20× lens. At least 5 images were collected for each individual muscle. Histological analyses were performed using Adobe Photoshop (Adobe, San Jose, CA, USA) to count all muscle fibers and all muscle cell nuclei in each image, while cross-sectional area was determined using ImageJ (NIH, Bethesda, MD, USA). To measure serum CK, blood was removed via cardiac puncture, and serum was collected by centrifugation at 10,000 rpm for 10 min. The colorimetric Serum Creatine Kinase Assay Kit (Abcam, Cambridge, MA, USA) was then used with a spectrophotometer to record enzymatic activity following the manufacturer's instructions.

Gastrocnemius force

As shown in Figure S1, muscle physiology was determined as described previously for WT gastrocnemius muscles.[69] WT mice treated RO with high doses of A6.C8hF were examined 5 and 10 weeks post treatment. Untreated age-matched mice were also examined as controls.

Treadmill fatigue analysis for WT mice

WT mice were acclimated to the treadmill (motorized Exer-3/6 shocker for mice and rats, Columbus Instruments) for 5 min at 10 m/s before each run. The speed was then increased at 1 m/s every minute until voluntary stoppage, which is when a mouse reacts to grid five times or spends a maximum 5 s sitting on the electrical grid at setting (0.7 mA, 200 ms/shock). This test was performed at 6, 10, and 14 weeks post injection.

Ankle torque plantar flexion

WT mice were anesthetized with isoflurane, and the lower right hindlimb was shaved. Mice were placed on a heated platform (37°C), and the foot of the mouse was attached to the lever of the servomotor (model 305; Aurora Scientific, Richmond Hill, ON, Canada) with the ankle joint at a 90° angle. Needle electrodes were inserted near the sciatic nerve and into the quadriceps of the right hindlimb to be stimulated at 10 mA. After initial measurements of maximum isometric twitch force and point of maximum tension were recorded, we performed a protocol consisting of 20 eccentric contractions at 100 Hz. The muscles were stimulated for 0.4 s per contraction, with 9-s rest intervals between measurements. The signal output of the force transducer was displayed on a storage oscilloscope (Tektronix Model 5111) coupled to a microcomputer used for data acquisition and storage. This test was performed on mice treated with A9.C8hF or AM.C8hF at 4, 8, and 12 weeks post injection.

Ultrasonography

Echocardiograms were performed on WT mice by the University of Washington Center for Translational Muscle Research core. Echocardiography was conducted with the Vevo 3100 high-frequency, high-resolution digital imaging system (VisualSonics). The mice were slightly anesthetized with 1%–1.5% isoflurane in oxygen. The parasternal short axis view at the mid-papillary level was used to obtain M-mode images for analysis of fractional shortening, ejection fraction, and other cardiac function parameters. Diastolic function was assessed by measurement of *trans*-mitral flow parameters from an apical 4-chamber view with pulsed-wave Doppler. Tissue Doppler imaging was performed by placing a sample volume at the septal corner of the mitral annulus. Mice were anesthetized by isoflurane and taped to a warmed platform (37°C). This test was performed at 6 and 12 weeks post injection.

TA force frequency

Prior to operative procedures, WT animals were anesthetized with isoflurane in an induction chamber and maintained under anesthesia using a nose cone during the procedure. A small incision to expose the distal tendon of the TA muscle was made. The intact tendon was tied to the lever arm of a servomotor (model 305-B, Aurora Scientific). The hindlimb was stabilized by pinning the knee and securing the foot to a heated platform (37°C). Needle electrodes were inserted on either side of the sciatic nerve. Stimulation voltage and muscle length were adjusted for maximum isomeric twitch force, and the optimal TA length was determined (L0). Tetanic twitch force was then measured at increasing stretch of L0: 0%, 5%, 10%, 15%, 20%, 25%, 30%, 35%, 40%, and 45%. The signal output of the force transducer was displayed on a storage oscilloscope (Tektronix model 5111) coupled to a microcomputer used for data acquisition and storage. Following the measurements of power, the muscle was isolated and

removed from the animal. The anesthetized animals were euthanized, and tissues were collected for histology and analysis.

Diaphragm force frequency

The diaphragm strip measurement began with whole-tissue removal while the mouse was under anesthesia. In a dissection bath (136.5 mM NaCl, 5 mM KCl, 1.8 mM $CaCl_2$, 0.5 mM $MgCl_2$, 0.4 mM NaH_2PO_4, and 11.9 mM $NaHCO_3$), sutures were tied around both ends of a small strip cut along the myofibers of the diaphragm. The strip was placed in a bath (121 mM NaCl, 5 mM KCl, 1.8 mM $CaCl_2$, 0.5 mM $MgCl_2$, 0.4 mM NaH_2PO_4, 24 mM $NaHCO_3$, and 5.5 mM glucose), and the sutures were tied to the servomotor (model 300-C, Aurora Scientific) and force transducer. A similar procedure as for the TA muscle strength assay was used, with the stimulation voltage and then muscle length adjusted for maximum isomeric twitch force, and the TA length was measured (L0). Tetanus (the point at which maximum tension is generated) was measured at increasing stretch of L0: 0%, 5%, 10%, 15%, 20%, 25%, 30%, 35%, 40%, and 45%. The signal output of the force transducer was displayed on a storage oscilloscope (Tektronix model 5111) coupled to a microcomputer used for data acquisition and storage.

Tissue collection and immunohistochemistry

At termination of the mice, the TA and heart were collected. Half of each muscle was positioned on OTC compound embedding medium for cryosectioning, while the other half plus the bilateral muscle of limbs were flash frozen in liquid nitrogen. The previously characterized mouse FKRP antiserum was used to visualize FKRP overexpression in cardiac and skeletal muscle cryosections.[45] Transverse and longitudinal 10-μm muscle sections were blocked in AffiniPure Fab fragment goat anti-mouse immunoglobulin G (IgG; 1:25 dilution, Jackson ImmunoResearch) diluted in 2% BSA for 1 h to prevent cross-reaction with endogenous mouse antibodies. Samples were washed in 1× PBS and incubated in primary antibodies at room temperature for 2 h. In addition to incubation with FKRP-C (1:200), samples were co-stained with organelle markers (BD Biosciences): GM130 (1:500), BiP/GRP78 (1:200), Bcl-2 (1:200), and EEA1 (1:250). Sections were washed in 1× PBS and re-blocked in 2% BSA for 10 min prior to secondary incubation with Alexa Fluor 488 goat anti-rabbit IgG (1:500, Molecular Probes) and Alexa Fluor 594 goat anti-mouse IgG1 or IgG2A (1:200, Molecular Probes). Samples were washed with 1× PBS prior to mounting with Fluoromount G (Southern Biotech).

Statistical analysis

Data are presented as means ± SEM, and statistical comparisons of non-parametric data points were made using Prism (GraphPad, La Jolla, CA, USA). Significant differences ($p \leq 0.05$ unless otherwise noted) were determined using a Student's t test or with a 1- or 2-way analysis of variance coupled to Tukey's post-hoc test for multiple mean comparisons. Significant differences are represented by different letters, and a shared letter indicates no difference. For example, three data points labeled a, ab, and b represent a significant difference between a and b because different letters indicate significance. There is no difference between a and ab or ab and b because they share letters.

DATA AVAILABILITY STATEMENT

Plasmids for the vectors described here must be obtained through a material transfer agreement (MTA) with the University of Washington. Details of the studies not clearly described can be obtained by contacting B.D.R. or J.S.C.

SUPPLEMENTAL INFORMATION

Supplemental information can be found online at https://doi.org/10.1016/j.omtm.2023.05.022.

ACKNOWLEDGMENTS

Supported by the LGMD2I Research Fund (to J.S.C., B.D.R., and D.C.L.), NIH R44AG079825 (to B.D.R.), NIH P30AR074990 (to M.R.), and NIH RO1AR040864 (to J.S.C.). AAV vectors were generated in the Sen. Paul D. Wellstone Muscular Dystrophy Specialized Research Center Viral Vector Core (NIH P50AR065139 to J.S.C.). We thank Qi Lu (McColl-Lockwood Laboratory for Muscular Dystrophy Research, Charlotte, NC, USA) and J.P. Laurent (LGMD2i Fund) for providing P448L mutant mice. Figure 1 was produced in BioRender.

AUTHOR CONTRIBUTIONS

H.B. conducted experiments, analyzed data, and wrote the initial manuscript. J.W.M., J.S., J.H., C.H., J.W., L.H., and N.P. conducted experiments and analyzed data. D.C.L. assisted with grant writing. Experimental planning and analysis. M.R., B.D.R., and J.S.C. assisted with grant writing, experimental planning, data analysis, and editing of the manuscript.

DECLARATION OF INTERESTS

The University of Washington has intellectual property rights to modified FKRP vector sequences as described here.

REFERENCES

1. Nickolls, A.R., and Bönnemann, C.G. (2018). The roles of dystroglycan in the nervous system: insights from animal models of muscular dystrophy. Dis. Model. Mech. *11*, dmm035931.

2. Ervasti, J.M., and Campbell, K.P. (1993). A role for the dystrophin-glycoprotein complex as a transmembrane linker between laminin and actin. J. Cell Biol. *122*, 809–823.

3. Praissman, J.L., Willer, T., Sheikh, M.O., Toi, A., Chitayat, D., Lin, Y.Y., Lee, H., Stalnaker, S.H., Wang, S., Prabhakar, P.K., et al. (2016). The functional o-mannose glycan on alpha-dystroglycan contains a phospho-ribitol primed for matriglycan addition. Elife *5*, e14473.

4. Mercuri, E., Brockington, M., Straub, V., Quijano-Roy, S., Yuva, Y., Herrmann, R., Brown, S.C., Torelli, S., Dubowitz, V., Blake, D.J., et al. (2003). Phenotypic spectrum associated with mutations in the fukutin-related protein gene. Ann. Neurol. *53*, 537–542.

5. Boito, C.A., Melacini, P., Vianello, A., Prandini, P., Gavassini, B.F., Bagattin, A., Siciliano, G., Angelini, C., and Pegoraro, E. (2005). Clinical and molecular characterization of patients with limb-girdle muscular dystrophy type 2i. Arch. Neurol. *62*, 1894–1899.

6. Sveen, M.L., Schwartz, M., and Vissing, J. (2006). High prevalence and phenotype-genotype correlations of limb girdle muscular dystrophy type 2i in Denmark. Ann. Neurol. *59*, 808–815.

7. Keramaris-Vrantsis, E., Lu, P.J., Doran, T., Zillmer, A., Ashar, J., Esapa, C.T., Benson, M.A., Blake, D.J., Rosenfeld, J., and Lu, Q.L. (2007). Fukutin-related protein localizes to the golgi apparatus and mutations lead to mislocalization in muscle in vivo. Muscle Nerve *36*, 455–465.

8. Esapa, C.T., McIlhinney, R.A.J., and Blake, D.J. (2005). Fukutin-related protein mutations that cause congenital muscular dystrophy result in er-retention of the mutant protein in cultured cells. Hum. Mol. Genet. *14*, 295–305.

9. Brockington, M., Blake, D.J., Prandini, P., Brown, S.C., Torelli, S., Benson, M.A., Ponting, C.P., Estournet, B., Romero, N.B., Mercuri, E., et al. (2001). Mutations in the fukutin-related protein gene (fkrp) cause a form of congenital muscular dystrophy with secondary laminin alpha2 deficiency and abnormal glycosylation of alpha-dystroglycan. Am. J. Hum. Genet. *69*, 1198–1209.

10. Tucker, J.D., Lu, P.J., Xiao, X., and Lu, Q.L. (2018). Overexpression of mutant fkrp restores functional glycosylation and improves dystrophic phenotype in fkrp mutant mice. Mol. Ther. Nucleic Acids *11*, 216–227.

11. Xu, L., Lu, P.J., Wang, C.H., Keramaris, E., Qiao, C., Xiao, B., Blake, D.J., Xiao, X., and Lu, Q.L. (2013). Adeno-associated virus 9 mediated fkrp gene therapy restores functional glycosylation of alpha-dystroglycan and improves muscle functions. Mol. Ther. *21*, 1832–1840.

12. Vannoy, C.H., Xiao, W., Lu, P., Xiao, X., and Lu, Q.L. (2017). Efficacy of gene therapy is dependent on disease progression in dystrophic mice with mutations in the fkrp gene. Mol. Ther. Methods Clin. Dev. *5*, 31–42.

13. Gicquel, E., Maizonnier, N., Foltz, S.J., Martin, W.J., Bourg, N., Svinartchouk, F., Charton, K., Beedle, A.M., and Richard, I. (2017). Aav-mediated transfer of fkrp shows therapeutic efficacy in a murine model but requires control of gene expression. Hum. Mol. Genet. *26*, 1952–1965.

14. Chan, Y.M., Keramaris-Vrantsis, E., Lidov, H.G., Norton, J.H., Zinchenko, N., Gruber, H.E., Thresher, R., Blake, D.J., Ashar, J., Rosenfeld, J., and Lu, Q.L. (2010). Fukutin-related protein is essential for mouse muscle, brain and eye development and mutation recapitulates the wide clinical spectrums of dystroglycanopathies. Hum. Mol. Genet. *19*, 3995–4006.

15. Blaeser, A., Awano, H., Wu, B., and Lu, Q.L. (2016). Progressive dystrophic pathology in diaphragm and impairment of cardiac function in fkrp p448l mutant mice. PLoS One *11*, e0164187.

16. Qiao, C., Wang, C.H., Zhao, C., Lu, P., Awano, H., Xiao, B., Li, J., Yuan, Z., Dai, Y., Martin, C.B., et al. (2014). Muscle and heart function restoration in a limb girdle muscular dystrophy 2i (lgmd2i) mouse model by systemic fkrp gene delivery. Mol. Ther. *22*, 1890–1899.

17. Krag, T.O., and Vissing, J. (2015). A new mouse model of limb-girdle muscular dystrophy type 2i homozygous for the common l276i mutation mimicking the mild phenotype in humans. J. Neuropathol. Exp. Neurol. *74*, 1137–1146.

18. Vannoy, C.H., Leroy, V., and Lu, Q.L. (2018). Dose-dependent effects of fkrp gene-replacement therapy on functional rescue and longevity in dystrophic mice. Mol. Ther. Methods Clin. Dev. *11*, 106–120.

19. Kregel, C.K., Allen, D.L., Booth, F.W., Fleshner, M.R., Henriksen, E.J., Musch, T.I., O'Leary, D.S., Parks, C.M., Poole, D.C., Ra'anan, A.W., et al. (2006). Resource Book for the Design of Animal Exercise Protocols (American Physiological Society).

20. De Luca, A. (2011). Use of treadmill and wheel exercise for impact on mdx mice phenotype. In TREAT-NMD Activity A07: Accelerate Preclinical Phase of New Therapeutic Treatment Development (TREAT-NMD Neuromuscular Network).

21. Grange, R.W. (2011). Use of treadmill and wheel exercise to assess dystrophic state. In TREAT-NMD Activity A07: Accelerate Preclinical Phase of New Therapeutic Treatment Development (TREAT-NMD Neuromuscular Network).

22. Bye, P.T., Esau, S.A., Walley, K.R., Macklem, P.T., and Pardy, R.L. (1984). Ventilatory muscles during exercise in air and oxygen in normal men. J. Appl. Physiol. *56*, 464–471.

23. Mahler, D.A., Moritz, E.D., and Loke, J. (1982). Ventilatory responses at rest and during exercise in marathon runners. J. Appl. Physiol. *52*, 388–392.

24. Bassett, D.R., Jr., and Howley, E.T. (2000). Limiting factors for maximum oxygen uptake and determinants of endurance performance. Med. Sci. Sports Exerc. *32*, 70–84.

25. Lindstedt, S.L., Thomas, R.G., and Leith, D.E. (1994). Does peak inspiratory flow contribute to setting vo2max? A test of symmorphosis. Respir. Physiol. *95*, 109–118.

26. Spurway, N.C., Ekblom, B., Noakes, T.D., and Wagner, P.D. (2012). What limits vo2max? A symposium held at the bases conference, 6 september 2010. J. Sports Sci. *30*, 517–531.

27. De Luca, A., Pierno, S., Liantonio, A., Cetrone, M., Camerino, C., Fraysse, B., Mirabella, M., Servidei, S., Rüegg, U.T., and Conte Camerino, D. (2003). Enhanced dystrophic progression in mdx mice by exercise and beneficial effects of taurine and insulin-like growth factor-1. J. Pharmacol. Exp. Therapeut. *304*, 453–463.

28. Okano, T., Yoshida, K., Nakamura, A., Sasazawa, F., Oide, T., Takeda, S., and Ikeda, S. (2005). Chronic exercise accelerates the degeneration-regeneration cycle and down-regulates insulin-like growth factor-1 in muscle of mdx mice. Muscle Nerve *32*, 191–199.

29. Rocco, A.B., Levalley, J.C., Eldridge, J.A., Marsh, S.A., and Rodgers, B.D. (2014). A novel protocol for assessing exercise performance and dystropathophysiology in the mdx mouse. Muscle Nerve *50*, 541–548.

30. Maricelli, J.W., Kagel, D.R., Bishaw, Y.M., Nelson, O.L., Lin, D.C., and Rodgers, B.D. (2017). Sexually dimorphic skeletal muscle and cardiac dysfunction in a mouse model of limb girdle muscular dystrophy 2i. J. Appl. Physiol. *123*, 1126–1138.

31. (2020). High-dose aav gene therapy deaths. Nat. Biotechnol. *38*, 910.

32. Wilson, J.M., and Flotte, T.R. (2020). Moving forward after two deaths in a gene therapy trial of myotubular myopathy. Hum. Gene Ther. *31*, 695–696.

33. Weinmann, J., Weis, S., Sippel, J., Tulalamba, W., Remes, A., El Andari, J., Herrmann, A.K., Pham, Q.H., Borowski, C., Hille, S., et al. (2020). Identification of a myotropic aav by massively parallel in vivo evaluation of barcoded capsid variants. Nat. Commun. *11*, 5432.

34. El Andari, J., Renaud-Gabardos, E., Tulalamba, W., Weinmann, J., Mangin, L., Pham, Q.H., Hille, S., Bennett, A., Attebi, E., Bourges, E., et al. (2022). Semirational bioengineering of aav vectors with increased potency and specificity for systemic gene therapy of muscle disorders. Sci. Adv. *8*, eabn4704.

35. Tabebordbar, M., Lagerborg, K.A., Stanton, A., King, E.M., Ye, S., Tellez, L., Krunnfusz, A., Tavakoli, S., Widrick, J.J., Messemer, K.A., et al. (2021). Directed evolution of a family of aav capsid variants enabling potent muscle-directed gene delivery across species. Cell *184*, 4919–4938.e22.

36. Lukowski, S.W., Bombieri, C., and Trezise, A.E.O. (2011). Disrupted post-transcriptional regulation of the cystic fibrosis transmembrane conductance regulator (cftr) by a 5'utr mutation is associated with a cftr-related disease. Hum. Mutat. *32*, E2266–E2282.

37. Lukowski, S.W., Rothnagel, J.A., and Trezise, A.E.O. (2015). Cftr mrna expression is regulated by an upstream open reading frame and rna secondary structure in its 5' untranslated region. Hum. Mol. Genet. *24*, 899–912.

38. Leppek, K., Das, R., and Barna, M. (2018). Functional 5' utr mrna structures in eukaryotic translation regulation and how to find them. Nat. Rev. Mol. Cell Biol. *19*, 158–174.

39. Cammas, A., and Millevoi, S. (2017). Rna g-quadruplexes: emerging mechanisms in disease. Nucleic Acids Res. *45*, 1584–1595.

40. Fay, M.M., Lyons, S.M., and Ivanov, P. (2017). Rna g-quadruplexes in biology: principles and molecular mechanisms. J. Mol. Biol. *429*, 2127–2147.

41. Salva, M.Z., Himeda, C.L., Tai, P.W., Nishiuchi, E., Gregorevic, P., Allen, J.M., Finn, E.E., Nguyen, Q.G., Blankinship, M.J., Meuse, L., et al. (2007). Design of tissue-specific regulatory cassettes for high-level raav-mediated expression in skeletal and cardiac muscle. Mol. Ther. *15*, 320–329.

42. Himeda, C.L., Chen, X., and Hauschka, S.D. (2011). Design and testing of regulatory cassettes for optimal activity in skeletal and cardiac muscles. Methods Mol. Biol. *709*, 3–19.

43. Gonçalves, M.A., Janssen, J.M., Nguyen, Q.G., Athanasopoulos, T., Hauschka, S.D., Dickson, G., and de Vries, A.A.F. (2011). Transcription factor rational design improves directed differentiation of human mesenchymal stem cells into skeletal myocytes. Mol. Ther. *19*, 1331–1341.

44. Martari, M., Sagazio, A., Mohamadi, A., Nguyen, Q., Hauschka, S.D., Kim, E., and Salvatori, R. (2009). Partial rescue of growth failure in growth hormone (gh)-deficient mice by a single injection of a double-stranded adeno-associated viral vector expressing the gh gene driven by a muscle-specific regulatory cassette. Hum. Gene Ther. *20*, 759–766.

45. Bengtsson, N.E., Seto, J.T., Hall, J.K., Chamberlain, J.S., and Odom, G.L. (2016). Progress and prospects of gene therapy clinical trials for the muscular dystrophies. Hum. Mol. Genet. *25*, R9–R17.

46. Hu, C., Kasten, J., Park, H., Bhargava, R., Tai, D.S., Grody, W.W., Nguyen, Q.G., Hauschka, S.D., Cederbaum, S.D., and Lipshutz, G.S. (2014). Myocyte-mediated arginase expression controls hyperargininemia but not hyperammonemia in arginase-deficient mice. Mol. Ther. *22*, 1792–1802.

47. Muir, L.A., Nguyen, Q.G., Hauschka, S.D., and Chamberlain, J.S. (2014). Engraftment potential of dermal fibroblasts following in vivo myogenic conversion in immunocompetent dystrophic skeletal muscle. Mol. Ther. Methods Clin. Dev. *1*, 14025.

48. Blankinship, M.J., Gregorevic, P., Allen, J.M., Harper, S.Q., Harper, H., Halbert, C.L., Miller, A.D., and Chamberlain, J.S. (2004). Efficient transduction of skeletal muscle using vectors based on adeno-associated virus serotype 6. Mol. Ther. *10*, 671–678.

49. Gao, G., Vandenberghe, L.H., Alvira, M.R., Lu, Y., Calcedo, R., Zhou, X., and Wilson, J.M. (2004). Clades of adeno-associated viruses are widely disseminated in human tissues. J. Virol. *78*, 6381–6388.

50. Alhamidi, M., Kjeldsen Buvang, E., Fagerheim, T., Brox, V., Lindal, S., Van Ghelue, M., and Nilssen, Ø. (2011). Fukutin-related protein resides in the golgi cisternae of skeletal muscle fibres and forms disulfide-linked homodimers via an n-terminal interaction. PLoS One *6*, e22968.

51. Gregorevic, P., Blankinship, M.J., Allen, J.M., Crawford, R.W., Meuse, L., Miller, D.G., Russell, D.W., and Chamberlain, J.S. (2004). Systemic delivery of genes to striated muscles using adeno-associated viral vectors. Nat. Med. *10*, 828–834.

52. Yin, F.C., Spurgeon, H.A., Rakusan, K., Weisfeldt, M.L., and Lakatta, E.G. (1982). Use of tibial length to quantify cardiac hypertrophy: application in the aging rat. Am. J. Physiol. *243*, H941–H947.

53. Kishimoto, T.K., and Samulski, R.J. (2022). Addressing high dose aav toxicity - 'one and done' or 'slower and lower. Expet Opin. Biol. Ther. *22*, 1067–1071.

54. Ertl, H.C.J. (2022). Immunogenicity and toxicity of aav gene therapy. Front. Immunol. *13*, 975803.

55. Mendell, J.R., Al-Zaidy, S.A., Rodino-Klapac, L.R., Goodspeed, K., Gray, S.J., Kay, C.N., Boye, S.L., Boye, S.E., George, L.A., Salabarria, S., et al. (2021). Current clinical applications of in vivo gene therapy with aavs. Mol. Ther. *29*, 464–488.

56. Bonnemann, C.G., Belluscio, B.A., Braun, S., Morris, C., and Muntoni, F. (2022). A collaborative analysis by clinical trial sponsors and academic experts of anti-transgene saes in studies of gene therapy for DMD. Mol. Ther. *30*, 4.

57. Cheng, A., Liu, C., Ye, W., Huang, D., She, W., Liu, X., Fung, C.P., Xu, N., Suen, M.C., Ye, W., et al. (2022). Selective c9orf72 g-quadruplex-binding small molecules ameliorate pathological signatures of als/ftd models. J. Med. Chem. *65*, 12825–12837.

58. Hordeaux, J., Buza, E.L., Jeffrey, B., Song, C., Jahan, T., Yuan, Y., Zhu, Y., Bell, P., Li, M., Chichester, J.A., et al. (2020). Microrna-mediated inhibition of transgene expression reduces dorsal root ganglion toxicity by aav vectors in primates. Sci. Transl. Med. *12*, eaba9188.

59. Cao, J., Novoa, E.M., Zhang, Z., Chen, W.C.W., Liu, D., Choi, G.C.G., Wong, A.S.L., Wehrspaun, C., Kellis, M., and Lu, T.K. (2021). High-throughput 5' utr engineering for enhanced protein production in non-viral gene therapies. Nat. Commun. *12*, 4138.

60. Wasala, N.B., Yue, Y., Vance, J., and Duan, D. (2017). Uniform low-level dystrophin expression in the heart partially preserved cardiac function in an aged mouse model of duchenne cardiomyopathy. J. Mol. Cell. Cardiol. *102*, 45–52.

61. Keramaris, E., Lu, P.J., Tucker, J., and Lu, Q.L. (2017). Expression of glycosylated alpha-dystroglycan in newborn skeletal and cardiac muscles of fukutin related protein (fkrp) mutant mice. Muscle Nerve *55*, 582–590.

62. Kregel, K.C., Allen, D.L., Booth, F.W., Fleshner, M.R., Henrikson, E.J., and Musch, T.I. (2006). Resource Book for the Design of Animal Exercise Protocols.

63. Konopka, A.R., and Harber, M.P. (2014). Skeletal muscle hypertrophy after aerobic exercise training. Exerc. Sport Sci. Rev. *42*, 53–61.

64. Gehrig, S.M., Koopman, R., Naim, T., Tjoakarfa, C., and Lynch, G.S. (2010). Making fast-twitch dystrophic muscles bigger protects them from contraction injury and attenuates the dystrophic pathology. Am. J. Pathol. *176*, 29–33.

65. Webster, C., Silberstein, L., Hays, A.P., and Blau, H.M. (1988). Fast muscle fibers are preferentially affected in duchenne muscular dystrophy. Cell *52*, 503–513.

66. Halbert, C.L., Allen, J.M., and Chamberlain, J.S. (2018). Aav6 vector production and purification for muscle gene therapy. Methods Mol. Biol. *1687*, 257–266.

67. Speakman, J.R. (2013). Measuring energy metabolism in the mouse - theoretical, practical, and analytical considerations. Front. Physiol. *4*, 34.

68. Maricelli, J.W., Bishaw, Y.M., Wang, B., Du, M., and Rodgers, B.D. (2018). Systemic smad7 gene therapy increases striated muscle mass and enhances exercise capacity in a dose-dependent manner. Hum. Gene Ther. *29*, 390–399.

69. Banks, G.B., and Chamberlain, J.S. (2008). The value of mammalian models for duchenne muscular dystrophy in developing therapeutic strategies. Curr. Top. Dev. Biol. *84*, 431–453.